Title: 2-^{18}F-Fluoroethanol is a novel positron emission tomography (PET) reporter of solid tumour perfusion.

Brennan J Wadsworth[1,2], Jinhe Pan[3], Iulia Dude[3], Nadine Colpo[3], Momir Bosiljcic[1,2], Kuo-Shyan Lin*[3], Francois Benard*[3], Kevin L Bennewith*[1,2]

*Co-senior authors
[1]Integrative Oncology, BC Cancer Agency, Vancouver, BC, Canada.
[2]Pathology and Laboratory Medicine, University of British Columbia, Vancouver, BC, Canada
[3]Molecular Oncology, BC Cancer Agency, Vancouver, BC, Canada.

Corresponding Author:
Dr. Kevin Bennewith
#10-108, 675 West 10th Ave,
Vancouver, British Columbia
Canada, V5Z1L3
Phone: 604-675-8042
Fax: 604-675-8049
Email: kbennewi@bccrc.ca

First Author:
Brennan Wadsworth, PhD candidate
Address: #9-202, 675 West 10th Ave, Vancouver, BC, Canada, V5Z 1L3
Phone: 604-675-8000 x7700
Email: bwadsworth@bccrc.ca

Word Count: 4991

Short Title: 2-^{18}F-FEtOH as a perfusion reporter

Key Words: positron emission tomography, tumour perfusion, 2-^{18}F-fluoroethanol, hydralazine, nicotinamide

Abstract

Solid tumour perfusion is a proven variable of interest for predicting cancer aggression and response to therapy. Current methods for non-invasively imaging tumour perfusion with positron emission tomography (PET) are limited by restricted accessibility and short half-lives of perfusion radiotracers. This study presents 2-^{18}F-fluoroethanol (2-^{18}F-FEtOH) as a perfusion reporter that can distinguish between tumours of varying perfusion levels and can be applied to screening drugs that modify tumour perfusion.

Methods: Uptake of 2-^{18}F-FEtOH in 4T1 and 67NR murine mammary carcinoma tumours grown in mice was measured using *ex vivo* radiography as well as static and dynamic PET imaging. 2-^{18}F-FEtOH uptake was directly compared with the ^{14}C-Iodoantipyrine perfusion reporter and perfusion-modifying drugs nicotinamide, pentoxifylline, and hydralazine were utilized to manipulate tumour perfusion before 2-^{18}F-FEtOH quantification.

Results: Uptake of 2-^{18}F-FEtOH in 4T1 and 67NR tumours was consistent with known perfusion differences within and between these tumours. 2-^{18}F-FEtOH uptake corresponded well with ^{14}C-Iodoantipyrine, and reflected the tumour perfusion modifying effects of each drug.

Conclusion: 2-^{18}F-FEtOH is a novel ^{18}F-based radiotracer for investigating tumour perfusion with PET imaging. Quantification of 2-^{18}F-FEtOH uptake can be used to distinguish between tumours of varying perfusion, and to screen the efficacy of blood flow modifying drugs for use as adjuvants to existing cancer therapies.

INTRODUCTION

Non-invasive imaging modalities are critical components of cancer care that can visualize the varied and widespread nature of cancer, and PET is a workhorse technique for non-invasive imaging. The utility of PET has evolved from detecting metabolically active tumours with 2-^{18}F-fluorodeoxyglucose towards a broader ability to characterize the tumour microenvironment. Within this trend are radiotracer indicators of tumour hypoxia (ie regions of low oxygen content), such as ^{18}F-fluoromisonidazole, ^{18}F-fluoroazomycin arabinoside, and ^{18}F-EF5. Tumour hypoxia is associated with reduced overall survival and poor prognosis in multiple cancer types(*1*) because hypoxic cells are resistant to therapy and exhibit multi-faceted support of metastasis(*2*). Successes of PET hypoxia reporters in patient studies include distinguishing aggressive high-grade glioblastoma multiform from less aggressive astrocytoma and oligodendrioma(*3*) as well as prediction of resistance to primary endocrine therapy in breast cancer(*4*).

Hypoxia develops in tumours from a combination of high metabolic demand and insufficient delivery of oxygenated blood. Tumour vasculature is typically abnormal, exhibiting low vascular density and a dysfunctional architecture prone to leakiness and regional perfusion loss(*5*). The fact that hypoxia develops in regions with insufficient perfusion creates a challenge for detecting tumour hypoxia via PET imaging due to concerns that the radiotracer may not have access to all hypoxic regions. Indeed, some reports in patients suggest that tumour regions with low perfusion are not always matched with high uptake of hypoxia reporters (*6,7*) despite the high likelihood of low regional oxygen content. Tumour perfusion itself is also a primary variable of interest, since tumour perfusion influences nutrient delivery to the tumour with potential effects

on tumour metabolism and progression, and tumour perfusion also affects delivery of chemotherapeutics. Measuring tumour perfusion either at baseline or before and after a therapy cycle has predicted disease free survival in patients with breast cancer[8,9], response to chemotherapy in head and neck cancer[10], response of cervical cancer to radiation therapy[11], and response of glioblastoma to anti-angiogenic therapy[12]. In addition to complementing hypoxia reporters and independently providing prognostic data, non-invasive imaging of tumour perfusion could be used pre-clinically to study strategies for modifying tumour perfusion for either radio-sensitization or manipulating chemotherapy delivery.

The gold standard in PET based imaging of perfusion is ^{15}O-H$_2$O (half-life: 2 minutes). The initial development of ^{15}O-H$_2$O was for myocardial perfusion imaging[13,14] and cerebral perfusion imaging[15], although ^{15}O-H$_2$O has recently been used for imaging tumour perfusion[6-8]. The main challenge with using ^{15}O-H$_2$O and other established PET reporters of perfusion with rapid half-lives, such as ^{15}O-butanol[16] and ^{13}N-NH$_3$[17] (half-life: 10 minutes), is the requirement of an on-site cyclotron for production and nearby administration. Rubidium-82 (^{82}Rb, half-life: 1.25 minutes) is a validated perfusion reporter[18] that can be produced using a ^{82}Sr/^{82}Rb generator, thus alleviating the need for an on-site cyclotron. However, ^{82}Rb suffers from a long positron range[19], which reduces PET resolution. ^{82}Rb also exhibits relatively low tissue extraction from the blood, at least in myocardium studies, which results in low contrast between well-perfused and poorly-perfused regions[20]. We believe that development of an ^{18}F (half-life: 110 minutes) based reporter of tumour perfusion will

provide both logistical and accessibility benefits, while possessing the shortest positron range (and therefore highest PET resolution) of the radioisotopes discussed[19].

This study presents 2-^{18}F-fluoroethanol (2-^{18}F-FEtOH) as a novel reporter of tumour perfusion. We have previously shown that 2-^{18}F-FEtOH indiscriminately labels well-perfused organs in the body, exhibits relatively low rates of defluorination, and provides a large window of time for imaging due to an extended plateau of activity that is protected from biological clearance[21]. This plateau is believed to arise from intracellular conversion of 2-^{18}F-FEtOH to ^{18}F-fluoroacetate followed by conversion to ^{18}F-fluoroacetylCoA and ^{18}F-fluorocitrate, both of which are trapped inside cells[22]. We predict that this 2-^{18}F-FEtOH-mediated accumulation of ^{18}F inside well-perfused cells will enhance contrast against poorly-perfused cells to provide strong resolution of intra-tumoural regional differences in perfusion status, and allow for imaging of tumour perfusion well after the injection of the radiotracer.

We aimed to validate 2-^{18}F-FEtOH as a reporter of tumour perfusion using PET in murine tumour models. We assessed if 2-^{18}F-FEtOH uptake would discriminate between tumours with differing perfusion phenotypes by using 67NR and 4T1 murine mammary carcinomas[23]. To determine if 2-^{18}F-FEtOH uptake is specific to perfusion status we conducted direct comparison to the established perfusion reporter ^{14}C-iodoantipyrine (^{14}C-IAP)[24], we conducted kinetic analysis of dynamic PET scans to ensure 2-^{18}F-FEtOH uptake was dependent on plasma input, and we manipulated tumour perfusion with the blood flow modifying agents nicotinamide, pentoxifylline, and hydralazine. Our data indicate that 2-^{18}F-FEtOH is a novel radiotracer applicable to quantifying native or drug-induced changes in tumour perfusion by PET.

METHODS

2-^{18}F-FEtOH synthesis

2-^{18}F-FEtOH was synthesized as described previously(*21*).

^{18}F Gamma Counting and ^{14}C Liquid Scintillation Counting

^{14}C-Iodoantipyrine and 2-^{18}F-FEtOH were co-injected into anesthetized mice, which were sacrificed 2 minutes post-injection for tissue harvest. Harvested tissue was subject to gamma counting for detection of ^{18}F activity using a Wizard2 2480 automatic gamma counter (Perkin Elmer) followed by ^{14}C counting using a RackBeta1219 liquid scintillation counter (LKB Wallac).

Mouse Tumour Models

10 week old female BALB/c mice were purchased from Taconic (Germantown, NY) and housed in the Animal Resource Centre at the BC Cancer Agency Research Centre under specific pathogen-free conditions. 67NR and 4T1 murine mammary carcinoma cell lines (gifts from Dr. Fred Miller, Karmanos Cancer Institutes, Detroit, MI) were maintained in RPMI 1640 medium + 10% FBS and used within 20 passages. All animal experiments were performed in accordance with Institutional and Canadian Council on Animal Care guidelines.

Antibodies

Tumour sections were stained with unconjugated CD31 antibody (BD Pharmingen) with Alexa 594 secondary antibody (Invitrogen), and FITC-conjugated antibody against pimonidazole (Hypoxyprobe). 100mg/kg pimonidazole was injected intraperitoneally 1.5

hours prior to mouse sacrifice. Images were captured with a Retiga EXi camera (QImaging) using an Axiovert S100 microscope (Carl Zeiss Canada).

Ex Vivo Radiography Experiments

Mice received tail vein injections of 20 MBq 2-^{18}F-FEtOH followed 55 minutes later by tail vein injection of 50 µL of 10 mg/mL Hoechst 33342 (Thermo Fisher Scientific). Drug treated mice received either 500 mg/kg nicotinamide (Sigma-Aldrich) 30 min prior to 2-^{18}F-FEtOH, or 10 mg/kg hydralazine (Sigma-Aldrich) or 50 mg/kg pentoxifylline (Sigma-Aldrich) 15 min prior to 2-^{18}F-FEtOH. Tumours were harvested and immediately embedded in OCT, sectioned onto microscope slides, and incubated on a phosphor screen for 90 min before detection using a Typhoon FLA 9500 scanner (GE Life Sciences).

Phosphor images were analyzed using ImageJ software. Activity histograms were gathered from regions of interest drawn around individual tumours. The line profile function on ImageJ was used to quantify regional differences in 2-^{18}F-FEtOH activity. This tool returns the pixel intensity at each point along a line drawn across the full width of each tumour radiography image. To quantify the presence of central ischemia, the intensity of ^{18}F activity at the centre of each tumour was calculated as the average of the 11 pixels closest to the mid-point of each line. Tumour-centre intensity values were divided by the maximum intensity value of the entire tumour to express the tumour-centre values as a fraction of the maximum. Three line profiles were drawn and data averaged for each tumour image.

PET Imaging Experiments

PET imaging was conducted as previously published *(21)*. Rate of irreversible 2-^{18}F-FEtOH uptake was determined with the Patlak method *(25)* using image-derived input functions from the vena cava as previously published *(26)* and analysis conducted with MatLab software (MathWorks).

RESULTS

2-^{18}F-FEtOH Uptake Depicts Regional Perfusion Differences Within Tumours

Immunofluorescent images of 67NR and 4T1 (Fig 1A) tumours grown orthotopically in contralateral mammary fat pads show distinct phenotypes of vascular density and blood vessel function. CD31 vascular endothelium staining was significantly more prevalent in 67NR than in 4T1 tumours (Fig 1B; 10.01±0.71% vs 4.43±0.23% mean± standard error of the mean (SEM)), indicating greater vascular density in 67NR tumours. We also assessed uptake of intravenously administered Hoechst 33342 fluorescent dye, which diffuses out of perfused blood vessels to intercalate into cellular DNA. Nearly twice as much tumour area stained positive for Hoechst 33342 in 67NR vs 4T1 tumours (Fig 1B; 10.30±0.65% vs 5.79±0.56% mean±SEM) indicating that 67NR tumour blood vessels are relatively well-perfused. Consistently, we observed greater staining of the exogenous hypoxia reporter pimonidazole in 4T1 tumours than in 67NR tumours (Fig 1B; 23.06±2.55% vs 0.45±0.15% mean±SEM). Overall the 4T1 tumours were found to exhibit low blood vessel density, poor perfusion, and large amounts of hypoxia, which opposes their syngeneic counterpart 67NR tumours and agrees with past research *(27,28)*.

The microenvironment of 4T1 tumours provides a model for assessing regional perfusion differences due to the common presence of necrosis in the centre of these tumours. The centres of 4T1 tumours are poorly perfused and do not contain viable tissue, as indicated by a lack of Hoechst 33342 staining (Fig 2A). This is again in contrast to 67NR tumours that display perfusion throughout the tumour (Fig 2A). We exploited this feature as a first test for 2-^{18}F-FEtOH as a reporter of tumour perfusion, hypothesizing that the radiotracer would be present only in the periphery of 4T1 tumours and throughout 67NR tumours.

Ex vivo radiography of 2-^{18}F-FEtOH conducted on tumours excised 55 minutes post-injection displayed similar patterns to Hoechst 33342; low activity was observed in central regions of 4T1 tumours, moderate activity in the periphery of 4T1 tumours, and high activity throughout 67NR tumours (Fig 2B). To quantify these observations, the pixel intensities were assessed in line profiles drawn across the width of each tumour's radiography image (eg Supplemental Fig 1). Values of the 11 pixels closest to the midpoint of the line profile were averaged to represent the 2-^{18}F-FEtOH activity in the tumour centre. These values were compared to the maximum intensity in the entire associated tumour image. We observed that pixel intensities in the centre of 67NR tumours were 88±2.0% the value of the maximum 67NR intensity, while the centre of 4T1 tumours were only 65±5.7% of their tumour maximums (Fig 2C). These results suggest that 2-^{18}F-FEtOH uptake provides intra-tumoural resolution of perfusion status that is in agreement with blood vessel density, perfusion status, and hypoxia in 4T1 and 67NR tumours.

2-^{18}FEtOH Uptake Agrees with Validated Perfusion Reporter ^{14}C-Iodoantipyrine

To link 2-^{18}F-FEtOH uptake with tissue perfusion, we co-injected 2-^{18}F-FEtOH with ^{14}C-IAP, which is a validated perfusion reporter used to study cerebral and tumour perfusion(29-31) by measuring *ex vivo* ^{14}C-IAP activity. We found that 2-^{18}F-FEtOH and ^{14}C-IAP radioactivity in brain tissue and in 67NR and 4T1 tumours provided clear distinction of each tissue type, with a general progression from poorly perfused 4T1 tumours through 67NR tumours, and up to well perfused brain tissue. 2-^{18}F-FEtOH and ^{14}C-IAP activities were significantly correlated, and the dynamic range of 2-^{18}F-FEtOH activity was greater than ^{14}C-IAP with a slope of 1.162±0.1416 %ID/g across all tissues analyzed (Fig 3).

2-^{18}F-FEtOH Provides Distinction Between 67NR and 4T1 Tumours for an Extended Period of Time

We measured 2-^{18}F-FEtOH uptake in 67NR and 4T1 tumours for 55 minutes post-injection using dynamic PET imaging. Based upon previous work showing stable uptake of 2-^{18}F-FEtOH into cells(22), we hypothesized that 2-^{18}F-FEtOH activity would reach plateaus reflective of tumour perfusion status. In baseline scans, 2-^{18}F-FEtOH uptake into 67NR tumours plateaued at approximately 5.8%ID/g after 2 minutes and activity did not significantly change over the remaining protocol (Fig 4A). 2-^{18}F-FEtOH activity in 4T1 tumours did not reach a plateau until 30 minutes post-injection at approximately 4.5%ID/g, after which no further increase was observed (Fig 4A). 2-^{18}F-FEtOH activity in 67NR tumours was significantly greater than 4T1 from 1 minute until 12 minutes post-injection (Fig 4A). We performed static PET scans 55 minutes post-injection of 2-^{18}F-FEtOH to further assess this late time point in mice not anesthetized during tracer uptake (Fig 4B). Pairwise assessment of mean 2-^{18}F-FEtOH activity in

each tumour revealed greater activity in 67NR versus the same-mouse 4T1 tumours in eleven out of twelve mice (Fig 4C). Further analysis computed static PET data into cumulative frequency plots (Supplemental Fig 2A) to calculate the 2-^{18}F-FEtOH activity level representative of the 50th and 90th voxel percentiles. Results showed that both the 50th and 90th percentile activity levels were greater in the 67NR tumours (Supplemental Fig 2B; 7.75±0.18%ID/g vs 6.58±0.31%ID/g, and 9.29±0.19%ID/g vs 7.71±0.23%ID/g, mean±SEM $p < 0.05$). These data confirm that the 2-^{18}F-FEtOH radiotracer successfully distinguishes 67NR and 4T1 tumours using dynamic PET imaging or static PET imaging, including the potential for 2-^{18}F-FEtOH to report perfusion for a longer period of time compared to previously published PET-based perfusion reporters.

Irreversible Uptake Rate of 2-^{18}F-FEtOH is Dependent on Perfusion and Not Tumour Line

We hypothesized that 2-^{18}F-FEtOH is irreversibly taken up into cells, fitting with a two tissue compartment model. While this allows for the signal stability displayed in Figure 4, it poses the risk of having 2-^{18}F-FEtOH uptake select for cells and tissues better able to metabolize FEtOH. To address this concern we conducted Patlak modeling(*25*) of 2-^{18}F-FEtOH uptake into 67NR and 4T1 tumours using image-derived input functions (Supplemental Fig 3) based on voxels of ^{18}F activity derived from dynamic PET images of the mouse vena cava(*26*) after injection of 2-^{18}F-FEtOH. The Patlak method outputs an irreversible uptake rate constant 'Ki' that is dependent on both metabolism of the radiotracer and its concentration in the plasma. Thus, Ki reflects possible intrinsic differences between cells and the delivery of 2-^{18}F-FEtOH through perfused vasculature. When Ki values were determined based on tissue activity curves

of full tumour volumes, the Ki was significantly greater in 67NR tumours than 4T1 tumours (1.6-fold difference, data not shown). However, regions of interest drawn selectively in well-perfused peripheral 4T1 regions produced similar Ki values as whole 67NR tumours (Fig 5). In contrast, the poorly-perfused center 4T1 regions possessed Ki values that were significantly lower than 67NR tumours or peripheral regions of 4T1 tumours. These data support that differences in 2-^{18}F-FEtOH uptake are due to perfusion differences and not differences in FEtOH metabolism.

2-^{18}F-FEtOH Uptake Into Tumours is Modified by Perfusion-Modifying Drugs

We next tested three blood flow modifying agents to observe if 2-^{18}F-FEtOH uptake into 4T1 and 67NR tumours would reflect the perfusion changes. We utilized two agents to increase tumour blood flow, nicotinamide(*32*) and pentoxifylline(*33*), and used hydralazine as an agent to reduce tumour blood flow(*34*) prior to *ex vivo* radiography of 2-^{18}F-FEtOH uptake from tumours harvested 55 minutes post-injection. Nicotinamide increased 2-^{18}F-FEtOH uptake in both 67NR and 4T1 tumours, indicated by the rightward shifts towards greater pixel intensity on histograms (Fig 6A,B). This is consistent with the known activity of nicotinamide to improve solid tumour perfusion. Similarly, pentoxifylline increased 2-^{18}F-FEtOH uptake in both tumours (Supplemental Fig 4A,B), with a more modest rightward shift compared to nicotinamide for either tumour type. Hydralazine induced a leftward shift in 4T1 tumour histograms (Fig 6A), indicating a reduction in perfusion that is consistent with the known activity of hydralazine. However, 67NR tumours did not display a reliable shift in response to hydralazine at this time point when tumours were harvested 55 minutes after 2-^{18}F-FEtOH injection (Fig 6B).

To further investigate the responses of 67NR and 4T1 tumours to hydralazine, we performed dynamic PET imaging of 2-^{18}F-FEtOH uptake after hydralazine administration compared to baseline images (sample images in Supplemental Fig 5). 67NR tumours treated with hydralazine displayed a significant reduction in 2-^{18}F-FEtOH activity over the first 10 minutes of dynamic PET imaging (Fig 7A). 67NR 2-^{18}F-FEtOH activity in control and hydralazine groups converged within 55 minutes, agreeing with the *ex vivo* radiography data (Fig 6B). The mean 2-^{18}F-FEtOH activity in 4T1 tumours was reduced throughout the dynamic scan (Fig 7B). These data indicate that dynamic imaging is required to accurately assess the changes in tumour perfusion induced by blood flow modifying drugs.

DISCUSSION

This study presents 2-^{18}F-FEtOH as a novel radiotracer for measuring tumour perfusion. We have found that uptake of 2-^{18}F-FEtOH is dependent on regional perfusion status, with 2-^{18}F-FEtOH uptake in agreement with the intra-tumoural heterogeneity of Hoechst 33342 staining (Fig 2). 2-^{18}F-FEtOH uptake also accurately reflected the perfusion statuses of two tumour models with distinct vascular and hypoxic phenotypes (Fig 1-4). 2-^{18}F-FEtOH uptake into 67NR and 4T1 tumours, and brain tissue displayed strong agreement with the validated perfusion reporter ^{14}C-IAP, while 2-^{18}F-FEtOH uptake displayed a greater dynamic range in distinguishing each tissue (Fig 3).

We also show that 2-^{18}F-FEtOH uptake can be used to measure the effects of pharmacological agents that modify tumour perfusion (Fig 6,7). We tested two vasoactive drugs (nicotinamide and hydralazine) as well as pentoxifylline, which

increases perfusion by improving the flexibility of red blood cells to facilitate their flow through tortuous tumour vessels(35,36). Further experiments with hydralazine displayed that assessing the effects of perfusion-modifying agents is aided by time course analyses such as dynamic PET imaging (Fig 7). Taken together, our data show the potential for 2-^{18}F-FEtOH uptake quantified by dynamic PET imaging to be used to screen blood flow-modifying agents for use as therapeutic adjuvants to existing cancer therapies.

The extended half life of the ^{18}F isotope provides 2-^{18}F-FEtOH with the benefits of accessibility and eased protocol timelines compared with [15]O radiotracers. 2-^{18}F-FEtOH is also stably taken up into cells and produces an activity plateau in well-perfused tissue as measured previously in many healthy tissues(21). An extended half life and activity plateau provides a unique opportunity to detect perfusion at later time points post-injection, with activity plateaus lasting up to 30 minutes and later time points exhibiting only a small increase in activity (Fig 4,7).

The data displayed in this study presents the utility of 2-^{18}F-FEtOH as a general indicator of tumour perfusion, distinguishing well-perfused and poorly perfused regions. To support that perfusion is the driving factor in 2-^{18}F-FEtOH uptake in this study and not cellular differences in metabolic trapping, we applied the Patlak method to determine the irreversible uptake rate constant Ki. The value of Ki is reflective of both the concentration of 2-^{18}F-FEtOH delivered to a tissue and the ability for the tissue to metabolize the radiotracer into cell impermeable metabolites. In this study, Ki values did not vary between 67NR tumours and well-perfused regions of 4T1 tumours in the same animal (Fig 5). Rather, Ki values varied strongly within 4T1 tumours in a regional

manner, with the lowest Ki values associated with 4T1 tumour centres (Fig 5), which we also showed to be poorly perfused (Fig 2). These modeling data are somewhat limited by the use of an image derived input function instead of direct blood draws to assess 2-^{18}F-FEtOH in the bloodstream, although image analysis methods have fared well when directly compared to blood collection methods(26). Future kinetic modelling of 2-^{18}F-FEtOH should include analysis of FEtOH metabolites and assessment of enzymes that will relate to enhanced metabolic trapping.

Future studies should evaluate 2-^{18}F-FEtOH uptake as a measure of tumour perfusion in other solid tumour types. Of additional interest will be investigating the oxygenation of tumour regions with low 2-^{18}F-FEtOH activity to distinguish between poorly perfused and poorly oxygenated tumour regions. Of additional interest is comparison of 2-^{18}F-FEtOH perfusion and PET-based hypoxia measurements to predict patient response to radiation therapy and particularly chemotherapy, where other perfusion reporters have provided strong prognostic data on tumour response. The accessibility benefit of 2-^{18}F-FEtOH over [15]O perfusion reporters and the ability to image 2-^{18}F-FEtOH 55 minutes post-injection would also make 2-^{18}F-FEtOH an appealing candidate to monitor tumour response during therapy to determine how tumour perfusion responds to therapy. Previous work showing 2-^{18}F-FEtOH uptake in normal tissues(21) suggest that 2-^{18}F-FEtOH-based perfusion measurements may have applicability beyond solid tumours, with potential for measuring tissue perfusion in other disease states. Taken together, our data support the further development and application of 2-^{18}F-FEtOH as a PET-based marker of tissue and solid tumour perfusion.

CONCLUSIONS

2-^{18}F-FEtOH is a novel PET reporter of perfusion. 2-^{18}F-FEtOH displays intra-tumour resolution of perfusion, discriminates well-perfused and poorly perfused tumours, responds to tumour-perfusion modifying pharmaceuticals, and provides an extended window of detection compared to current PET perfusion reporters.

Disclosure

No conflicts of interest are disclosed.

References:

1.	Vordermark D, Horsman MR. Hypoxia as a biomarker and for personalized radiation oncology. *Recent Results Cancer Res.* 2016;198:123–142.

2.	Bennewith KL, Dedhar S. Targeting hypoxic tumour cells to overcome metastasis. *BMC Cancer.* 2011;11:504.

3.	Hirata K, Terasaka S, Shiga T, et al. ^{18}F-Fluoromisonidazole positron emission tomography may differentiate glioblastoma multiforme from less malignant gliomas. *Eur J Nucl Med Mol Imaging.* 2012;39:760–770.

4.	Cheng J, Lei L, Xu J, et al. 18F-Fluoromisonidazole PET/CT: A potential tool for predicting primary endocrine therapy resistance in breast cancer. *J Nucl Med.* 2013;54:333–340.

5.	Dewhirst M, Cao Y, Moeller B. Cycling hypoxia and free radicals regulate angiogenesis and radiotherapy response. *Nat Rev Cancer.* 2008;8:425–437.

6.	Bruehlmeier M, Roelcke U, Schubiger PA. Assessment of hypoxia and perfusion in human brain tumors using PET with 18F-fluoromisonidazole and 15O-H2O. *J Nucl Med.* 2004;45:1851-1859.

7.	Lehtiö K, Oikonen V, Grönroos T, et al. Imaging of blood flow and hypoxia in head and neck cancer: initial evaluation with [(15)O]H(2)O and [(18)F]fluoroerythronitroimidazole PET. *J Nucl Med.* 2001;42:1643–1652.

8.	Dunnwald LK, Gralow JR, Ellis GK, et al. Tumor metabolism and blood flow changes by positron emission tomography: relation to survival in patients treated with neoadjuvant chemotherapy for locally advanced breast cancer. *J Clin Oncol.* 2008;26:4449–4457.

9.	Humbert O, Riedinger J-MM, Vrigneaud J-MM, et al. 18F-FDG PET derived tumor blood flow changes after one cycle of neoadjuvant chemotherapy predicts outcome in triple-negative breast cancer. *J Nucl Med.* 2016;57:1707-1712.

10.	Bernstein JM, Kershaw LE, Withey SB, et al. Tumor plasma flow determined by dynamic contrast-enhanced MRI predicts response to induction chemotherapy in head and neck cancer. *Oral Oncol.* 2015;51:508–513.

11.	Huang Z, Yuh KA, Lo SS, et al. Validation of optimal DCE-MRI perfusion threshold to classify at-risk tumor imaging voxels in heterogeneous cervical cancer for outcome prediction. *Magn Reson Imaging.* 2014;32:1198–1205.

12.	Sorensen AG, Emblem KE, Polaskova P, et al. Increased survival of glioblastoma patients who respond to antiangiogenic therapy with elevated blood perfusion. *Cancer Res.* 2012;72:402–407.

13.	Herrero P, Markham J, Bergmann SR. Quantitation of myocardial blood flow with H2 15O and positron emission tomography: assessment and error analysis of a mathematical approach. *J Comput Assist Tomogr.* 1989;13:862–873.

14.	Bergmann SR, Fox KA, Rand AL, McElvany KD. Quantification of regional myocardial blood flow in vivo with H215O. *Circulation.* 1984;70:724-733.

15.   Frackowiak RS, Lenzi GL, Jones T, Heather JD. Quantitative measurement of regional cerebral blood flow and oxygen metabolism in man using 15O and positron emission tomography: theory, procedure, and normal values. *J Comput Assist Tomogr*. 1980;4:727–736.

16.   Berridge MS, Adler LP, Nelson AD, et al. Measurement of human cerebral blood flow with [15O]butanol and positron emission tomography. *J Cereb Blood Flow Metab*. 1991;11:707–715.

17.   Schelbert HR, Phelps ME, Huang SC, et al. N-13 ammonia as an indicator of myocardial blood flow. *Circulation*. 1981;63:1259–1272.

18.   Huang SC, Williams BA, Krivokapich J, Araujo L, Phelps ME, Schelbert HR. Rabbit myocardial 82Rb kinetics and a compartmental model for blood flow estimation. *Am J Physiol*. 1989;256:H1156–H1164.

19.   Cal-González J, Herraiz JL, España S, Desco M, Vaquero J, Udías J. Positron range effects in high resolution 3D PET imaging. *IEEE Nucl Sci Symp Conf Rec.* 2009:2788–2791.

20.   Maddahi J. Properties of an ideal PET perfusion tracer: new PET tracer cases and data. *J Nucl Cardiol*. 2012;19:S30–S37.

21.   Pan J, Pourghiasian M, Hundal N, et al. f-[18F]fluoroethanol and 3-[18F]fluoropropanol: facile preparation, biodistribution in mice, and their application as nucleophiles in the synthesis of [18F]fluoroalkyl aryl ester and ether PET tracers. *Nucl Med Biol*. 2013;40:850–857.

22.   Tewson TJ, Welch MJ. Preparation and preliminary biodistribution of" no carrier added" fluorine1-8 fluoroethanol. *J Nucl Med*. 1980;21:559–564.

23.   Aslakson, Miller. Selective events in the metastatic process defined by analysis of the sequential dissemination of subpopulations of a mouse mammary tumor. *Cancer Res*. 1992;52:1399–1405.

24.   Horton RW, Pedley TA, Meldrum BS. Regional cerebral blood flow in the rat as determined by particle distribution and by diffusible tracer. *Stroke*. 1980;11:39–44.

25.   Patlak CS, Blasberg RG. Graphical evaluation of blood-to-brain transfer constants from multiple-time uptake data. Generalizations. *J Cereb Blood Flow Metab*. 1985;5:584–590.

26.   Lanz B, Poitry-Yamate C, Gruetter R. Image-derived input function from the vena cava for 18F-FDG PET studies in rats and mice. *J Nucl Med*. 2014;55:1380–1388.

27.   Dexter DL, Kowalski HM, Blazar BA, Fligiel Z, Vogel R. Heterogeneity of tumor cells from a single mouse mammary tumor. *Cancer Res*. 1978;38:3174-3181

28.   Lou Y, McDonald P, Oloumi A, et al. Targeting tumor hypoxia: suppression of breast tumor growth and metastasis by novel carbonic anhydrase IX inhibitors. *Cancer Res*. 2011;71:3364–3376.

29.   Wang Z, Stefanko D, Guo Y, et al. Evidence of functional brain reorganization on the basis of blood flow changes in the CAG140 knock-in mouse model of Huntington's disease. *Neuroreport*. 2016;27:632-639.

30.   Tozer GM, Shaffi KM. Modification of tumour blood flow using the hypertensive agent, angiotensin II. *Br J Cancer*. 1993;67:981–988.

31.   Tatsumi M, Yutani K, Kusuoka H, Nishimura T. Technetium-99m HL91 uptake as a tumour hypoxia marker: relationship to tumour blood flow. *Eur J Nucl Med*. 1999;26:91–94.

32.   Chaplin DJ, Horsman MR, Trotter MJ. Effect of nicotinamide on the microregional heterogeneity of oxygen delivery within a murine tumor. *J Natl Cancer Inst*. 1990;82:672–676.

33.   Bennewith KL, Durand RE. Drug-induced alterations in tumour perfusion yield increases in tumour cell radiosensitivity. *Br J Cancer*. 2001;85:1577–1584.

34.   Ljungkvist A, Bussink J, Rijken P, Raleigh J, Denekamp J, Kogel A. Changes in tumor hypoxia measured with a double hypoxic marker technique. *Int J Radiat Oncol Biol Phys*. 2000;48:1529–1538.

35.   Lee I, Levitt SH, Song CW. Improved tumour oxygenation and radiosensitization by combination with nicotinamide and pentoxifylline. *Int J Radiat Biol*. 1993;64:237–244.

36.   Ehrly AM. The effect of pentoxifylline on the flow properties of human blood. *Curr Med Res Opin*. 1978;5:608–613.
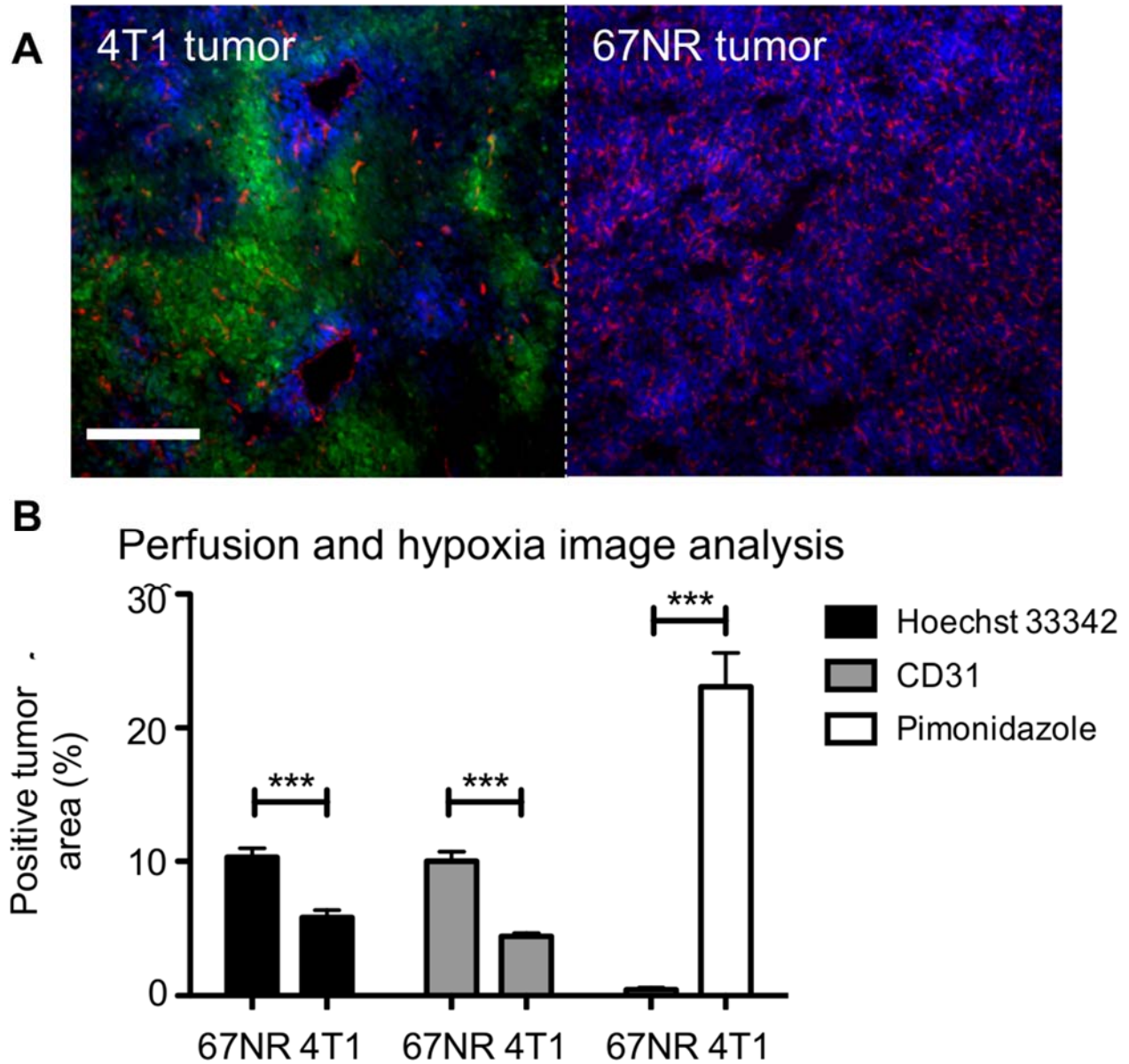
Figure 1. (A) Immunofluorescent images of 67NR and 4T1 tumours; perfusion indicated by hoechst 33342 (blue), vascular endothelium by CD31 (red), and hypoxia by pimonidazole (green). Scale bar 250μm. (B) Percent tumour area positive for Hoechst 33342, CD31, and pimonidazole (N=8, mean ± SEM, unpaired t-test, ***p<0.0001).
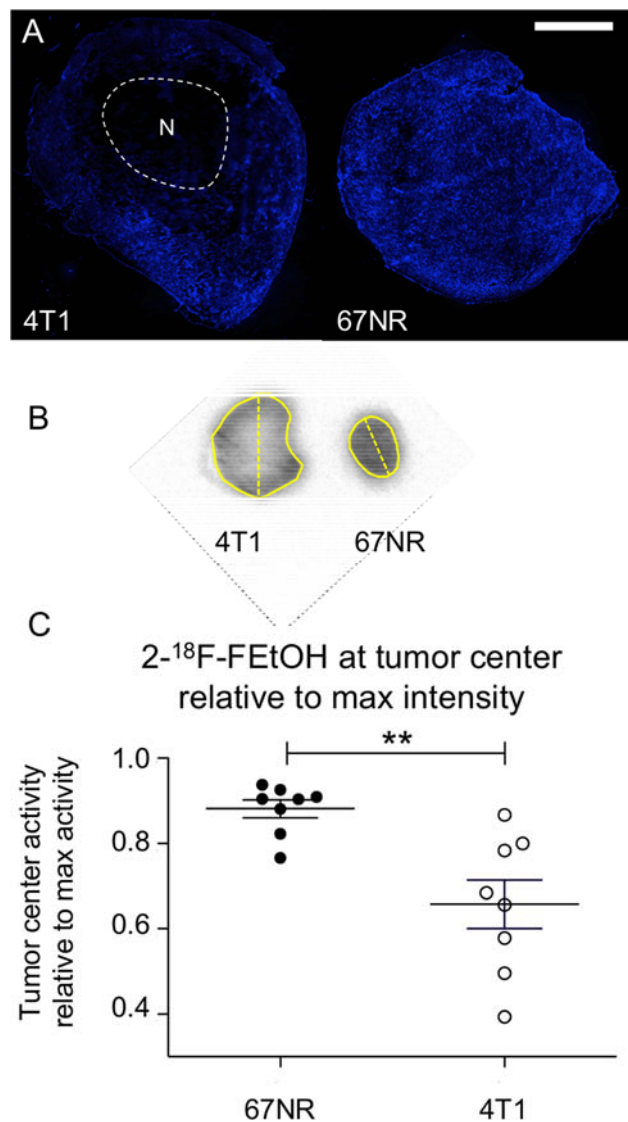
Figure 2. (A) Fluorescent microscopy of Hoechst 33342 in 4T1 and 67NR tumours, identifies central necrosis (N) in 4T1 tumours. Scale bar 250 μm. (B) 2-^{18}F-FEtOH radiography of untreated tumours, solid yellow line defines tumour border, dashed lines are examples of where line profiles are drawn. (C) Tumour-centre ^{18}F intensity expressed relative to tumour-max intensity displays the low 2-^{18}F-FEtOH uptake in the centre of 4T1 tumours (N=7, t-test *p<0.05).
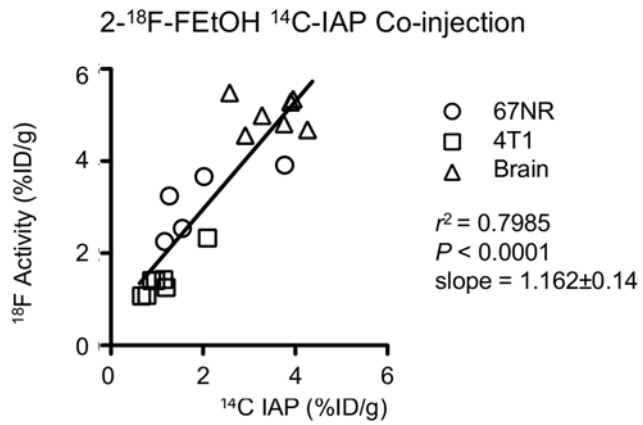
Figure 3. 2-^{18}F-FEtOH was co-injected with ^{14}C-IAP and bulk tissue radioactivity measured to determine uptake of each radiotracer. Linear regression trend line across all three tissues is displayed in black.
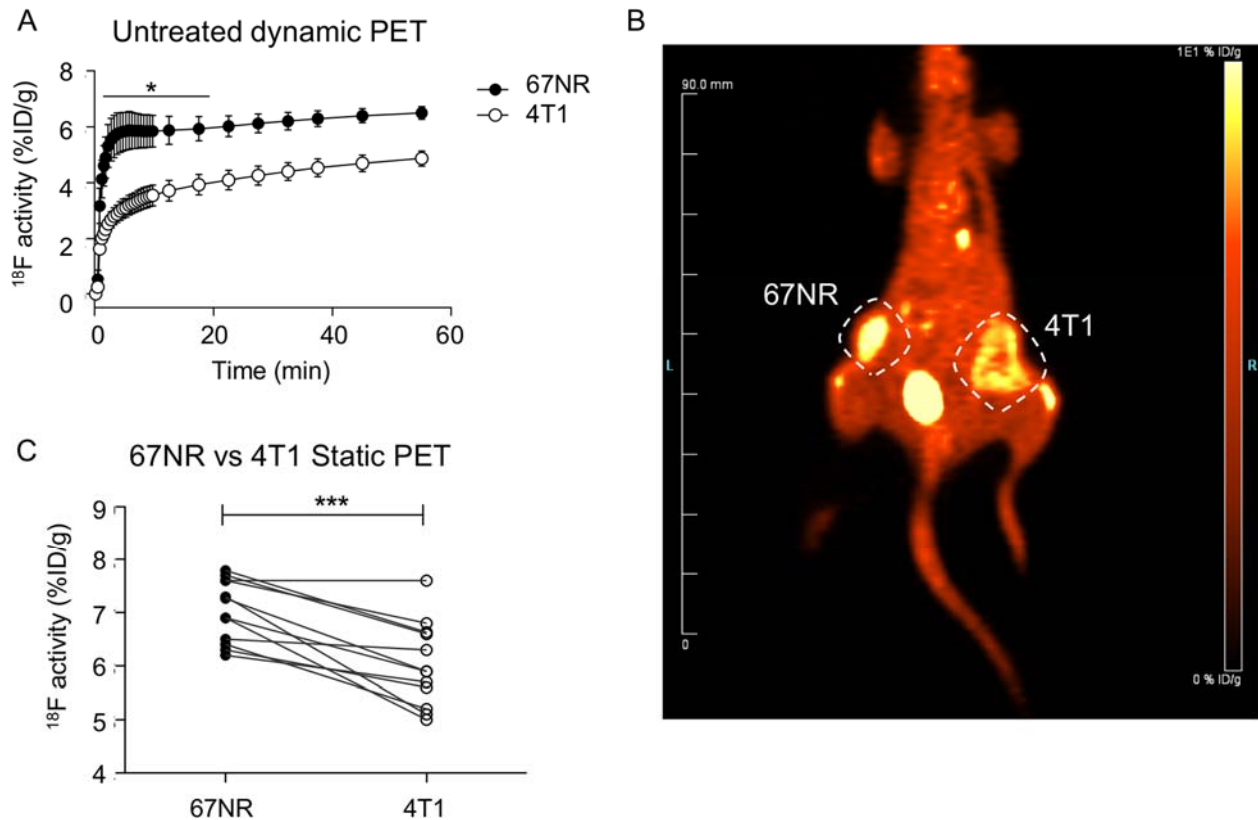
Figure 4. 2-^{18}F-FEtOH distinguishes 67NR from 4T1 tumours. (A) Mean tumour 2-^{18}F-FEtOH activity during dynamic PET (N=4, mean ± SEM, two-way ANOVA with Bonferroni multiple comparisons 67NR vs 4T1 *p<0.05). (B) Sample whole body static PET image 55 minutes post-injection. (C) Mean tumour 2-^{18}F-FEtOH activity from static PET (N=12, paired t-test ***p<0.0001).
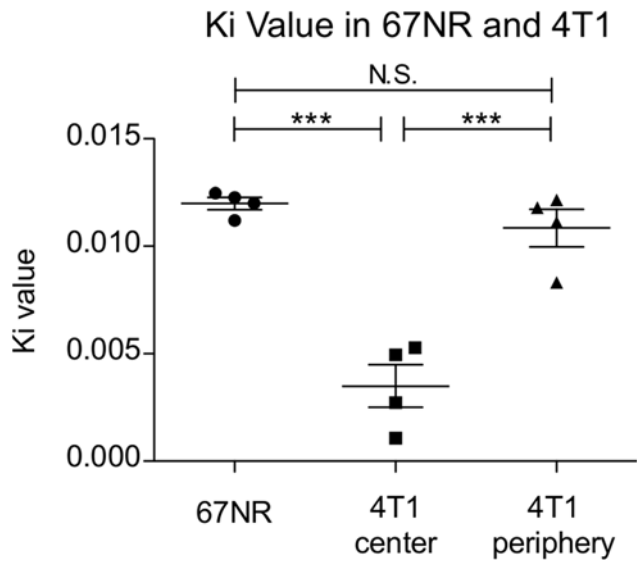
Figure 5. Patlak irreversible rate constant 'Ki' was computed for whole 67NR tumour volumes and compared to select regions of 4T1, the poorly-perfused tumour center and well-perfused periphery. (N=4, one-way ANOVA with tukey multiple comparisons test, ***p<0.0001)
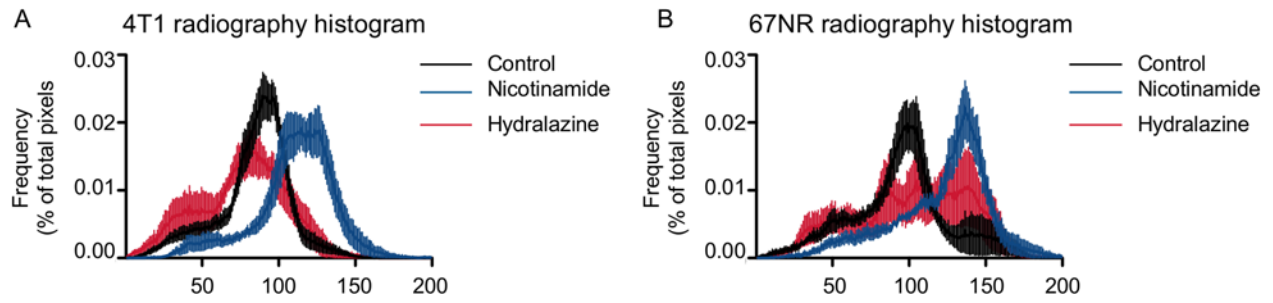
Figure 6. Perfusion modifying drugs alter 2-^{18}F-FEtOH uptake into (A) 4T1 and (B) 67NR tumours. Mice were administered one of nicotinamide or hydralazine prior to 2-^{18}F-FEtOH injection. Radioactivity was detected using radiography and expressed as histograms. (N=5, mean ± SEM).
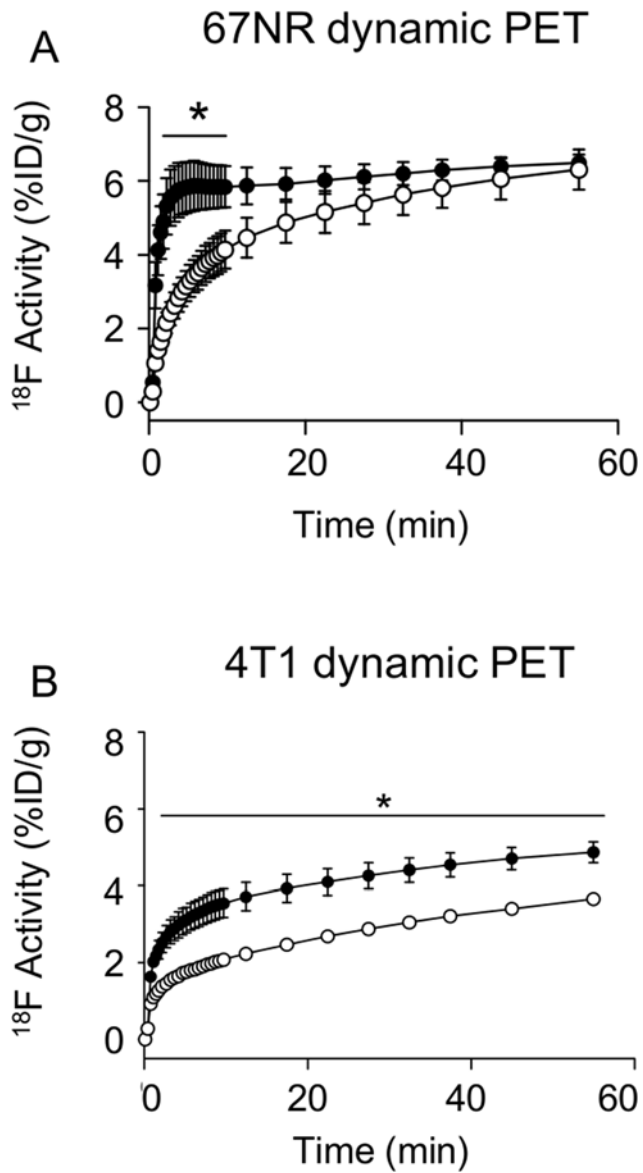
Figure 7. Hydralazine slows 2-^{18}F-FEtOH delivery. 2-^{18}F-FEtOH mean activity over dynamic PET comparing baseline (closed circles) scans and hydralazine (open circles) scans for (A) 67NR and (B) 4T1. (N=4, mean ± SEM, Bonferroni multiple comparisons *$p < 0.05$).

Supplementary Data:

Supplemental Figure 1. Sample line profile data for 67NR and 4T1 tumours from the

radiography images displayed in Figure 2.
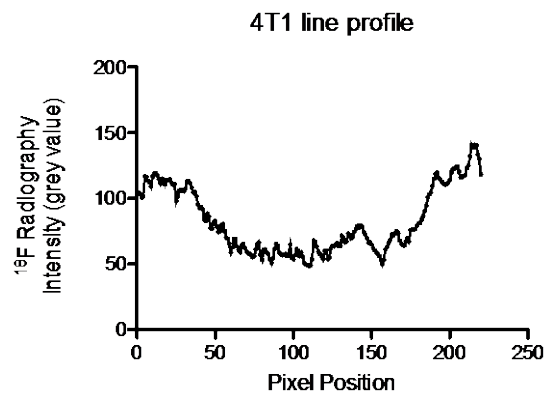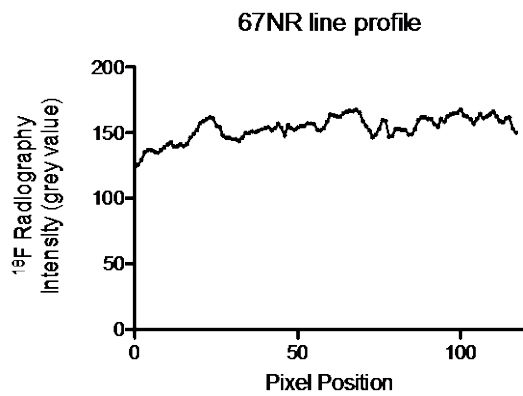
Supplemental Figure 2. (A) Cumulative frequency plots of static PET scans conducted 55 minutes post-injection of 2-^{18}F-FEtOH. Data display that 4T1 tumours voxel intensities are shifted left towards reduced radioactivity detected. This is quantified in (B) by comparing the 50th and 90th percentiles, both of which are significantly lower activity in 4T1 tumours.
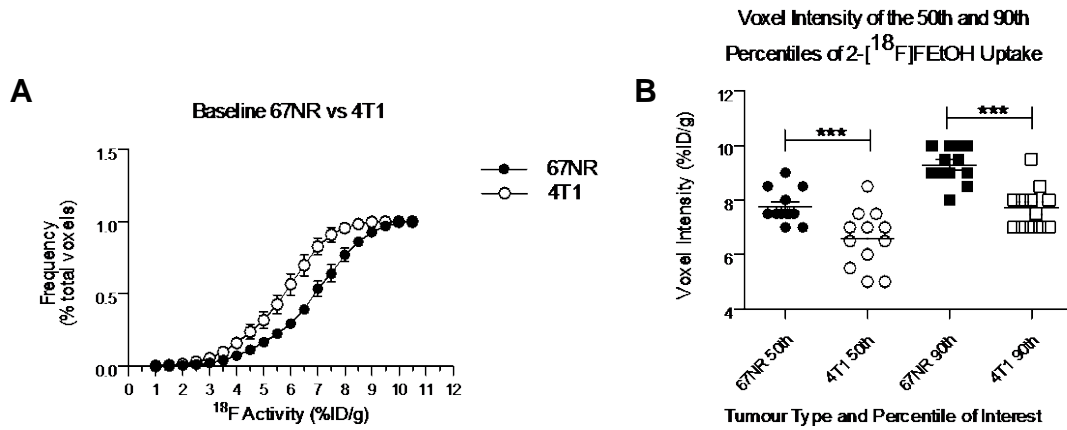
Supplementary Figure 3. Image derived input functions were produced based on the voxels within the Vena Cava, identified during the first pass of the 2-^{18}F-FEtOH bolus after the tail vein injection. Displayed is the input function averaged across four dynamic scans from untreated mice. Data points were produced every 5 seconds across the first 2 minutes, then every 30 seconds up until 5 minutes post-injection, and finally every 5 minutes until the end of the 60 minute PET scan.
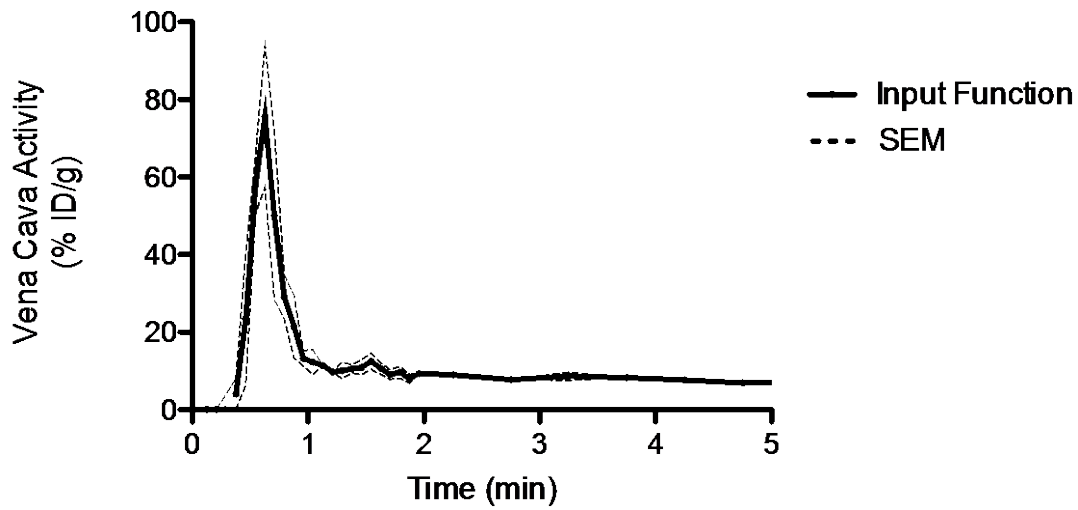
Supplemental Figure 4. Pentoxifylline shifted 4T1 (A) and 67NR (B) 2-^{18}F-FEtOH

radiography histograms towards increased radioactivity, consistent with the understood

effect of pentoxifylline to increase tumour perfusion.
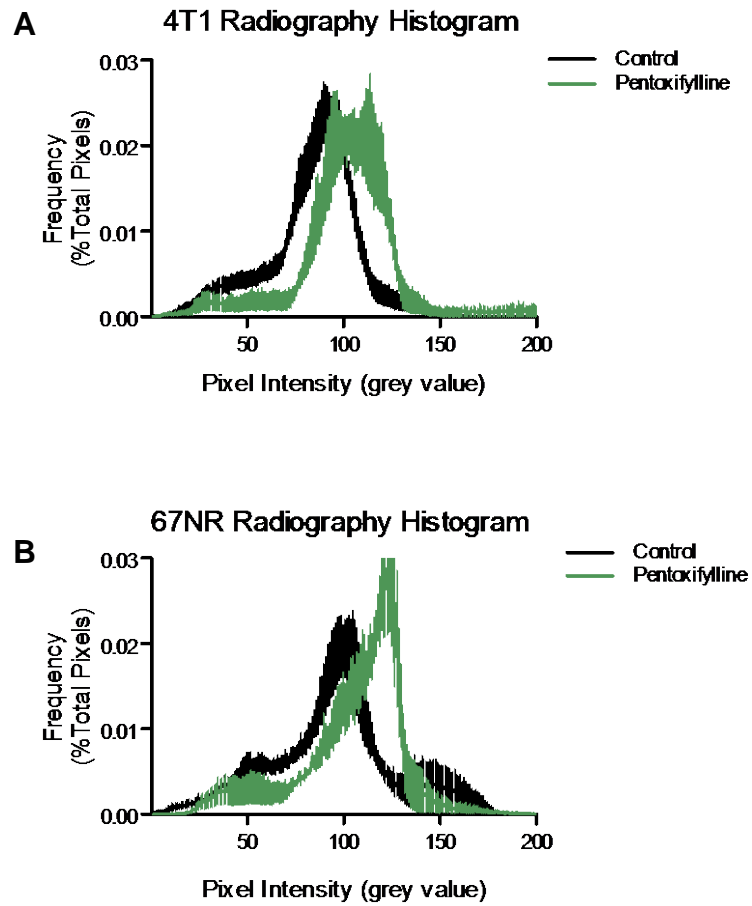
Supplemental Figure 5. Representative images from dynamic PET scans of the same mouse imaged for untreated baseline images (A) on the first day, and hydralazine pre-treatment (B). Images left to right are 1 minute post-injection of 2-^{18}F-FEtOH, 10 minutes post-injection, and 55 minutes post-injection.
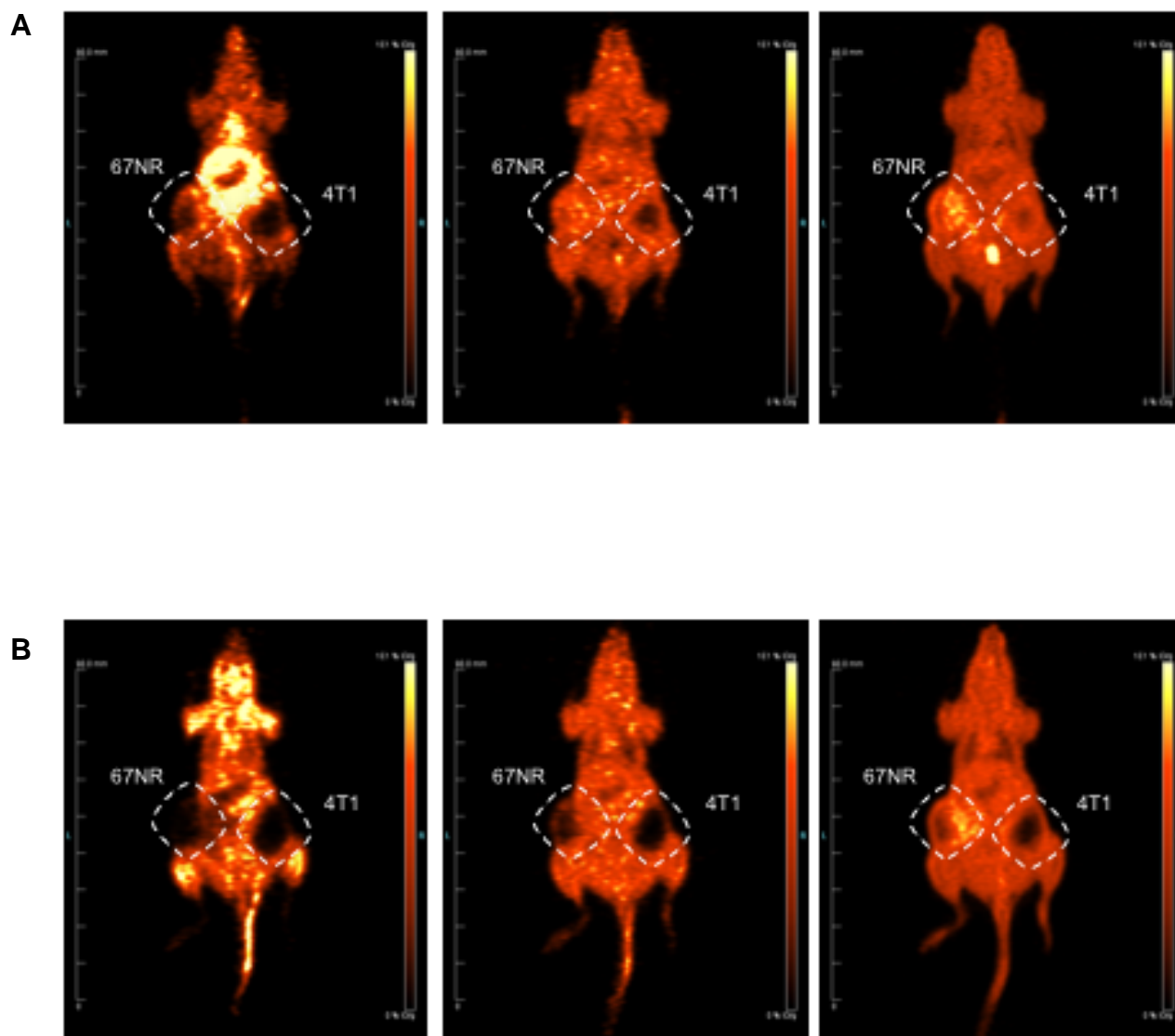
Supplemental Figure 6. Hydralazine induces an increase in skeletal muscle 2-^{18}F-FEtOH activity consistent with the 'steal effect'. Further, we observed a complete inhibition of 2-^{18}F-FEtOH clearance to the bladder in hydralazine treated mice, consistent with the fluid-retention effect of hydralazine.